JACS
JOURNAL OF THE AMERICAN CHEMICAL SOCIETY

Article

pubs.acs.org/JACS

Mechanistic Insights into Tunable Metal-Mediated Hydrolysis of Amyloid-β Peptides

Jeffrey S. Derrick,[†] Jiwan Lee,[‡] Shin Jung C. Lee,[†] Yujeong Kim,[§,∥] Eunju Nam,[†] Hyeonwoo Tak,[⊥] Juhye Kang,[†] Misun Lee,[†] Sun Hee Kim,[*,§,∥] Kiyoung Park,[*,‡] Jaeheung Cho,[*,⊥] and Mi Hee Lim[*,†]

[†]Department of Chemistry, Ulsan National Institute of Science and Technology (UNIST), Ulsan 44919, Republic of Korea
[‡]Department of Chemistry, Korea Advanced Institute of Science and Technology (KAIST), Daejeon 34141, Republic of Korea
[§]Western Seoul Center, Korea Basic Science Institute (KBSI), Seoul 03759, Republic of Korea
[∥]Department of Chemistry and Nano Science, Ewha Womans University, Seoul 03760, Republic of Korea
[⊥]Department of Emerging Materials Science, Daegu Gyeongbuk Institute of Science and Technology (DGIST), Daegu 42988, Republic of Korea

Supporting Information

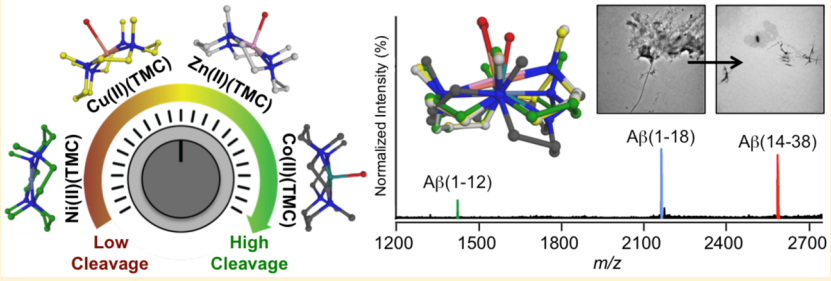

ABSTRACT: An amyloidogenic peptide, amyloid-β (Aβ), has been implicated as a contributor to the neurotoxicity of Alzheimer's disease (AD) that continues to present a major socioeconomic burden for our society. Recently, the use of metal complexes capable of cleaving peptides has arisen as an efficient tactic for amyloid management; unfortunately, little has been reported to pursue this strategy. Herein, we report a novel approach to validate the hydrolytic cleavage of divalent metal complexes toward two major isoforms of Aβ (Aβ_{40} and Aβ_{42}) and tune their proteolytic activity based on the choice of metal centers (M = Co, Ni, Cu, and Zn) which could be correlated to their anti-amyloidogenic properties. Such metal-dependent tunability was facilitated employing a tetra-*N*-methylated cyclam (TMC) ligand that imparts unique geometric and stereochemical control, which has not been available in previous systems. Co(II)(TMC) was identified to noticeably cleave Aβ peptides and control their aggregation, reporting the first Co(II) complex for such reactivities to the best of our knowledge. Through detailed mechanistic investigations by biochemical, spectroscopic, mass spectrometric, and computational studies, the critical importance of the coordination environment and acidity of the aqua-bound complexes in promoting amide hydrolysis was verified. The biological applicability of Co(II)(TMC) was also illustrated via its potential blood-brain barrier permeability, relatively low cytotoxicity, regulatory capability against toxicity induced by both Aβ_{40} and Aβ_{42} in living cells, proteolytic activity with Aβ peptides under biologically relevant conditions, and inertness toward cleavage of structured proteins. Overall, our approaches and findings on reactivities of divalent metal complexes toward Aβ, along with the mechanistic insights, demonstrate the feasibility of utilizing such metal complexes for amyloid control.

INTRODUCTION

A comprehensive understanding of the etiology of Alzheimer's disease (AD), the most common form of dementia, is still elusive even after more than a century of research. The consequence of our inability to unravel the intricacies of AD pathology has directly impeded the design and development of effective strategies against the disorder.[1−5] As a result, the numbers affected by AD have continued to rise.[6] Thus, to reverse this trend, more significant efforts to decipher the disease etiology and modes of actions of existing preventative strategies must be made.[1]

Since senile plaques predominately composed of amyloid-β (Aβ), an aggregation-prone peptide known to assemble into distinctive fibrillar structures, have been identified as a hallmark of AD (in the AD-affected brain, two amyloidogenic peptides, Aβ_{40} and Aβ_{42}, exist at ca. 90% and 9%, respectively; Aβ_{42} is more aggregation-prone than Aβ_{40}), a wealth of data has accumulated implicating it as a key contributor to neurodegeneration.[1−5,7−9] Unfortunately, a molecular-level understanding has yet to be resolved. Traditionally, small molecule

Received: September 15, 2016
Published: January 18, 2017

DOI: 10.1021/jacs.6b09681
J. Am. Chem. Soc. 2017, 139, 2234−2244

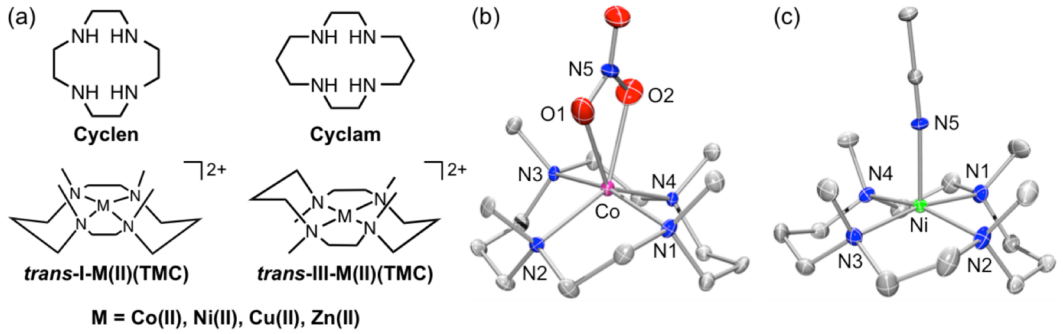

Figure 1. Chemical structures of macrocyclic polyamines and their metal complexes. (a) Chemical structures of cyclen, cyclam, and M(II)(TMC) (*trans*-I and *trans*-III isomers). Cyclen = 1,4,7,10-tetraazacyclododecane; cyclam = 1,4,8,11-tetraazacyclotetradecane; TMC = 1,4,8,11-tetramethyl-1,4,8,11-tetraazacyclotetradecane. ORTEP diagrams of (b) $[Co(TMC)(NO_3)](NO_3)$ and (c) $[Ni(TMC)(CH_3CN)](NO_3)_2$ with ellipsoids drawn at the 30% probability level. Non-coordinated nitrate anions and hydrogen atoms are omitted for clarity. Selected distances (Å) and angles are summarized in Tables S1–S3.

inhibitors have been used to prevent Aβ aggregation.[1,3,4,7,8] As a new approach, the utilization of transition metal complexes able to modulate Aβ aggregation has recently emerged.[7−16] The capacity of metal complexes to access various oxidation states, coordination numbers, and stereochemistry can further endow singular approaches as well as provide a degree of tunability, which is not easily achieved in small molecules.[7−16] One such approach to amyloid management is the cleavage of Aβ's amide bonds to produce peptide fragments that generate off-pathway and less toxic species. Co(III)(cyclen) derivatives (Figure 1) have been reported to hydrolyze the unactivated amide bonds in Aβ and other non-amyloidogenic and biologically essential proteins.[7,17−20] Unfortunately, apart from a single study, very little has been conducted to understand and utilize this approach for amyloid management.[19] For example, in an effort to achieve some degree of selectivity, more than 800 Co(III)(cyclen) derivatives augmented with exotic organic linkers were generated; however, only two complexes exhibited cleavage activity.[19] This synthetically cumbersome tactic identifies our limited comprehension of this methodology and thus retards our ability to rationally design effective metal complexes for peptide cleavage. Instead of using and evaluating such metal complexes, these macrocyclic polyamine ligands (i.e., cyclen and cyclam; Figure 1) have been mostly employed as exogenous metal chelators to combat metal-facilitated Aβ toxicity.[7,21−26] In addition to the inherent problems associated with metal chelation therapy in AD,[1] these ligands, due to the macrocyclic effect, possess high binding affinities and poor metal ion selectivity which may severely limit their biological applications.[7,21−26] Furthermore, unlike metal complexes composed of macrocyclic polyamine ligands, the *apo* ligands (i.e., cyclen and cyclam) are unable to modulate metal-free Aβ which also aggregates to produce toxic oligomers.[1,2,4,21,24−26] Therefore, it is clear that further studies are warranted into the application of metal macrocyclic polyamine complexes as proteolytic agents.

Herein, we report a novel approach to tune the hydrolytic cleavage activity of a series of divalent metal tetra-*N*-methylated cyclam complexes [M(II)(TMC); M = Co, Ni, Cu, and Zn; where M(II)(TMC) is used as an abbreviation] based on the choice of metal centers. Co(II)(TMC) was found to be the most effective agent for cleaving Aβ peptides and modulating their aggregation. Various techniques, such as mass spectrometry, electron paramagnetic resonance spectroscopy (EPR), X-ray crystallography, and density functional theory (DFT), were employed to establish mechanistic insights to explain Co(II)-(TMC)'s reactivity. The biological applicability of Co(II)-(TMC) was also indicated by its potential blood-brain barrier (BBB) permeability, relatively low cytotoxicity, regulatory activity against cytotoxicity triggered by Aβ, preferential cleavage of amyloidogenic proteins, as well as proteolytic reactivity under biologically relevant conditions. Taken together, our studies not only represent, to the best of our knowledge, the first Co(II) complex able to control Aβ aggregation via hydrolysis, along with the interaction with the peptide (e.g., complex formation), but also that the degree of excision to reactivity can easily be tuned through the choice of the metal center.

RESULTS

Design Rationale and Preparation of M(II)(TMC) Complexes. In order to probe the application of metal macrocyclic polyamine complexes as proteolytic and anti-amyloidogenic agents, a series of divalent metal tetramethylcyclam complexes, M(II)(TMC) (Figure 1a), were prepared following well-established methods.[27−33] TMC was chosen as the ligand for the metal complexes because of its distinctive stereochemistry (e.g., *trans*-I versus *trans*-III; Figure 1a) and coordination spheres (e.g., square planar, square pyramidal, trigonal bipyramidal (TBP), and octahedral geometries), as well as its accommodation of different oxidation and spin states of the metal centers.[27−33] We hypothesize that such properties of TMC may confer a certain degree of tunability in their interactions with Aβ that is absent in the octahedral Co(III)(cyclen) complexes.[23,27−33] In addition, M(II)(TMC) complexes can also be easily synthesized in high yields and modified via substitution reactions.[27]

Hydrolytic Cleavage of Aβ by M(II)(TMC) Complexes. In order to determine the ability of M(II)(TMC) to hydrolytically cleave both Aβ_{40} and Aβ_{42}, matrix-assisted laser desorption/ionization mass spectrometry (MALDI-MS) analyses were carried out (Figure 2). An immediate difference was noticeable in the MALDI-MS spectrum for the Aβ_{40} samples treated with Co(II)(TMC). The normalized signal intensity of the $A\beta_{40}^{+}$ monomer peak at 4328.15 m/z was noticeably reduced upon 24 h incubation with Co(II)(TMC) (Figure 2a). Similar monomer suppression was also observed for Aβ_{42} samples incubated with Co(II)(TMC) (Figure S1). Such a significant signal suppression of the $A\beta_{40}^{+}$ monomer was not

DOI: 10.1021/jacs.6b09681
J. Am. Chem. Soc. 2017, 139, 2234−2244

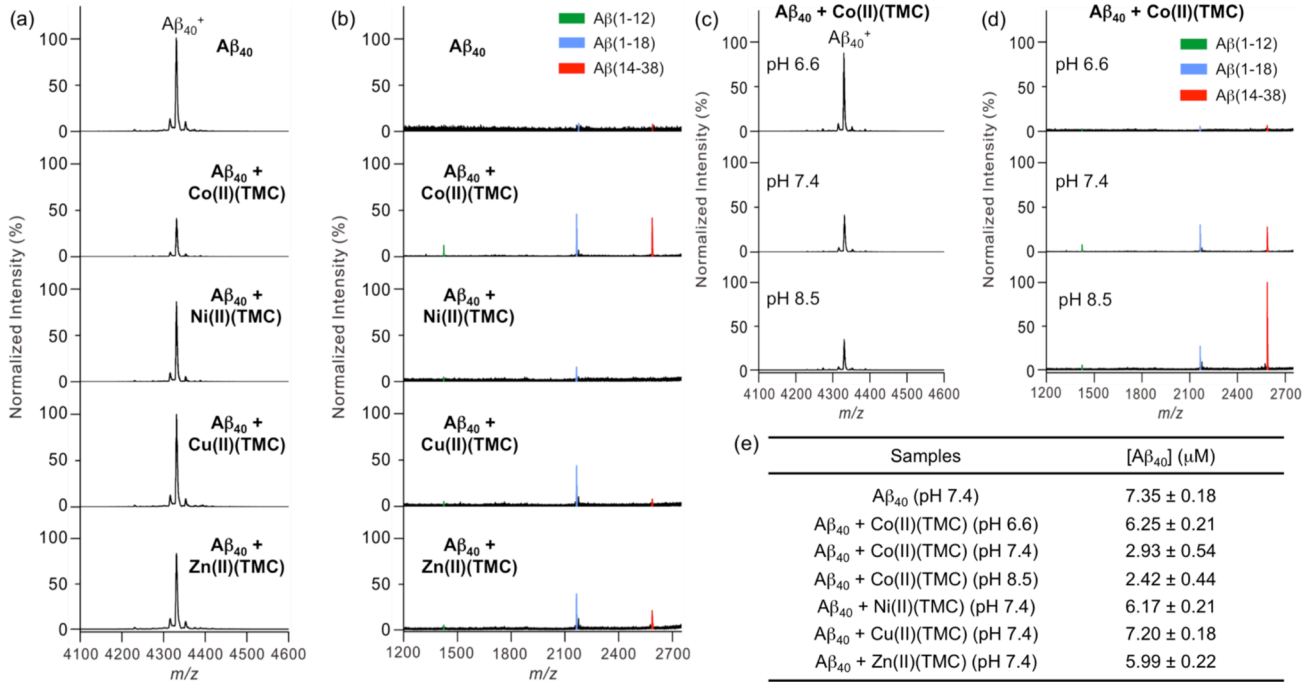

(e)

Samples	[$A\beta_{40}$] (μM)
$A\beta_{40}$ (pH 7.4)	7.35 ± 0.18
$A\beta_{40}$ + Co(II)(TMC) (pH 6.6)	6.25 ± 0.21
$A\beta_{40}$ + Co(II)(TMC) (pH 7.4)	2.93 ± 0.54
$A\beta_{40}$ + Co(II)(TMC) (pH 8.5)	2.42 ± 0.44
$A\beta_{40}$ + Ni(II)(TMC) (pH 7.4)	6.17 ± 0.21
$A\beta_{40}$ + Cu(II)(TMC) (pH 7.4)	7.20 ± 0.18
$A\beta_{40}$ + Zn(II)(TMC) (pH 7.4)	5.99 ± 0.22

Figure 2. MALDI-MS analysis of the $A\beta_{40}$ samples incubated with M(II)(TMC) (M = Co, Ni, Cu, and Zn). (a) Mass spectra of the singly charged $A\beta_{40}$. The peak intensities are normalized to $A\beta_{40}$ in the absence of M(II)(TMC). (b) The magnified low m/z range of the mass spectra. $A\beta(1-12)$ [m/z = 1424], $A\beta(1-18)$ [m/z = 2167], and $A\beta(14-38)$ [m/z = 2587] are indicated in light green, cyan, and red, respectively ($A\beta_{1-18}$ (ca. 64, 56, and 50 nM) from Ni(II)(TMC), Cu(II)(TMC), and Zn(II)(TMC), respectively). (c) MALDI-MS spectra for $A\beta_{40}$ incubated with Co(II)(TMC) at different pH values. The peak intensity is normalized to that of $A\beta_{40}$ without M(II)(TMC) (top spectrum). (d) Magnified spectrum (40x) for each sample. (e) The amount of the remaining singly charged $A\beta_{40}$ after M(II)(TMC) treatment is estimated and summarized in the table. All measurements were conducted with an internal standard, melittin (final concentration, 5 μM), and calibrated based on the linear correlation between the concentration and the signal intensity (Figure S2).

observed in the samples treated with Ni(II)(TMC), Cu(II)-(TMC), or Zn(II)(TMC) (Figure 2a).

To identify whether the $A\beta_{40}$ signal reduction was a result of a decrease in the monomeric $A\beta_{40}$ concentration upon incubation with Co(II)(TMC) or due to other factors, such as the aggregation of $A\beta$ or variation of $A\beta_{40}$ ionization efficiencies in the presence of Co(II)(TMC), we utilized an internal standard of melittin[34] to obtain quantitative information from the mass spectra. Through comparing the signal intensity of the internal standard in the $A\beta_{40}$ sample treated with Co(II)(TMC) to the $A\beta$ control we were able to verify that the $A\beta_{40}$ peak suppression was not due to differences in ionization efficiency and was most likely a result of a reduction in the monomeric, $A\beta_{40}^{+}$ concentration. To further elucidate the relative concentration of $A\beta_{40}^{+}$ with and without M(II)(TMC), a calibration plot was constructed utilizing the melittin internal standard in a concentration range of 50 nM–50 μM (R^2 = 0.99; Figure S2). As depicted in Figure 2e, while all M(II)(TMC) complexes caused a minor decrease in the concentration of $A\beta_{40}$, incubation with Co(II)(TMC) generated a much more significant reduction in the concentration of the $A\beta_{40}^{+}$ monomer (ca. 60% reduction; Figure 2a). Additionally, upon closer inspection of the low m/z range of the Co(II)(TMC)-treated mass spectrum, three new peaks were detected at 1424, 2167, and 2587 m/z, corresponding to the N- and C-terminal hydrolytic cleavage fragments, $A\beta_{1-12}$ (n.d.), $A\beta_{1-18}$ (ca. 53 nM), and $A\beta_{14-38}$ (ca. 42 nM), respectively (Figure 2b; "n.d." indicates not determined due to the detection limit). $A\beta$ monomer suppression and $A\beta$ fragmentation were also noticeably observed when two equivalents of Co(II)(TMC) were treated with the peptide showing increased peptide cleavage upon further addition of Co(II)(TMC) (Figure S3a–c). In the case of $A\beta_{42}$, similar fragmentation was also detected in the peptide sample incubated with Co(II)(TMC) (i.e., $A\beta_{4-10}$), but the signal intensity was much lower than that observed in the $A\beta_{40}$ samples (Figure S1). As shown in Figure S4a,b, the cleavage of $A\beta$ was not shown by Co(II)(EDTA), generated *in situ* by reacting $Co(NO_3)_2$ with EDTA (EDTA = ethylenediaminetetraacetic acid) in a ratio of 1:1, composed of the octahedral Co(II) center fully occupied by EDTA (no available site for H_2O binding). In addition, a cobalt salt (i.e., $Co(NO_3)_2$) could produce $A\beta$ fragments [e.g., $A\beta_{1-12}$ and $A\beta_{14-38}$] more noticeably, compared to Co(II)(TMC); however, its preference for cleavage sites in $A\beta$ was observed to be different from that of Co(II)(TMC) (Figure S4a,b). Moreover, as expected, no cleavage of $A\beta$ was indicated by the TMC ligand only. Thus, the observed proteolytic activity of Co(II)(TMC) toward $A\beta$ is identified to be originated by Co(II)(TMC) itself.

To further verify the hydrolytic mode of action for $A\beta$ cleavage, MALDI-MS samples of $A\beta_{40}$ incubated with Co(II)-(TMC) were prepared at different pHs (e.g., pH = 6.6, 7.4, and 8.5; Figure 2c–e).[18,19,35−39] Due to the high pH sensitivity of hydrolysis, we expected to observe significant differences in the $A\beta_{40}$ peak suppression and fragment signal intensity as the pH of the solution was altered with maximum cleavage occurring around neutral pH as has been reported for Co(III)(cyclen) complexes.[18,20,35,40] As expected, no significant fragmentation and very little $A\beta_{40}$ peak reduction were observed in the $A\beta_{40}$ samples incubated with Co(II)(TMC) for 24 h at pH 6.6

DOI: 10.1021/jacs.6b09681
J. Am. Chem. Soc. 2017, 139, 2234–2244

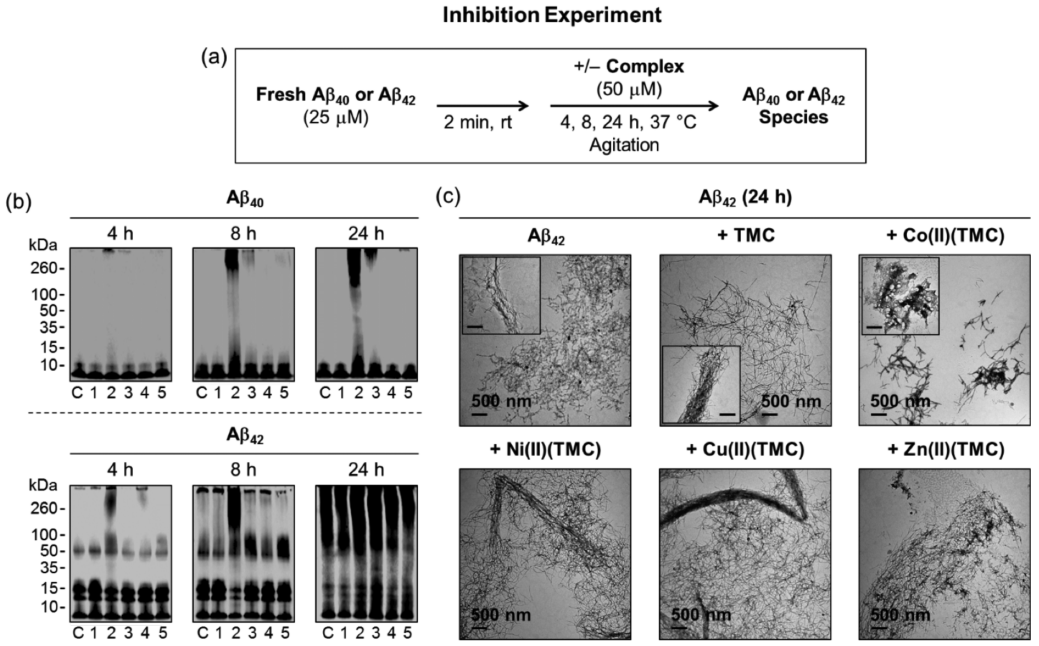

Figure 3. Capability of M(II)(TMC) (M = Co, Ni, Cu, and Zn) to control the aggregation pathways of Aβ_{40} and Aβ_{42}. (a) Scheme of the inhibition experiment. (b) Analysis of the resultant Aβ_{40} (top) and Aβ_{42} (bottom) species from the inhibition experiment, visualized by gel electrophoresis with Western blotting (gel/Western blot) using an anti-Aβ antibody (6E10). Conditions: Aβ (25 μM); M(II)(TMC) (50 μM); incubated for 4, 8, or 24 h; pH 7.4; 37 °C; constant agitation. Lanes: "C" denotes the control lane (without compound treatment); (1) Aβ + TMC; (2) Aβ + Co(II)(TMC); (3) Aβ + Ni(II)(TMC); (4) Aβ + Cu(II)(TMC); (5) Aβ + Zn(II)(TMC). (c) TEM images for the Aβ_{42} samples (24 h incubation) from (b). Insets represent the minor species.

(Figure 2c–e). Upon increasing the pH a noticeable difference in Co(II)(TMC)'s proteolytic activity was observed (Figure 2c–e). Through the use of the internal standard calibration plot we were able to determine that Co(II)(TMC) was slightly more reactive under moderately basic solution conditions (Figure 2c–e). In addition, the signal intensity of the Aβ_{14-38} fragment (2587 Da; ca. 155 nM) was highest in the pH 8.5 sample (Figure 2d; the Aβ_{1-18} fragment, ca. 55 nM). The overall pH dependence of Co(II)(TMC)'s cleavage activity supports its hydrolytic mechanism.

Effects of M(II)(TMC) on Aβ Aggregation. To evaluate the extent to which M(II)(TMC) complexes may modulate the aggregation pathways of both Aβ_{40} and Aβ_{42}, gel electrophoresis with Western blotting (gel/Western blot) and transmission electron microscopy (TEM) were employed to analyze the molecular weight (MW) distribution and morphology of the resultant Aβ species, respectively. Note that the quantitative analysis of M(II)(TMC) complexes' anti-amyloidogenic activity, assessed by fluorescence-based assays (e.g., thioflavin-T assay), was not obtained since they interfered with the assay leading to inaccurate results. Two different experiments were conducted to determine the ability of M(II)(TMC) complexes to either prevent the aggregation of monomeric Aβ (Figure 3a) or disassemble preformed Aβ fibrils into smaller species (Figure S5). Under our experimental conditions, compound-untreated samples assemble into large aggregates that can be visualized by TEM, but are too large to penetrate into the gel matrix thus producing very little smearing on the gel/Western blot (lane C, Figures 3 and S5). The administration of compounds, able to interact with Aβ and either (i) inhibit the formation of high MW aggregates and/or (ii) disassemble preformed aggregates, typically generates a distribution of smaller Aβ species that can enter into the gel inducing significant smearing compared to the samples containing Aβ only. It should be noted that the antibody, 6E10, used for gel/Western blot analysis is an N-terminal antibody, and therefore all of the hydrolyzed Aβ fragments may not have been detected on the gel/Western blots.

In inhibition experiments (Figure 3), a time-dependent change in the MW distribution of Aβ_{40} species was observed only for the samples treated with Co(II)(TMC). No smearing was discernible at the 4 h incubation; however, after 8 h, noticeable bands (ca. 10–15 and >260 kDa) were identified and darker and more significant smearing was detected upon further 24 h incubation (ca. 10–260 kDa; Figure 3b, top). The modulating effect of Co(II)(TMC) on Aβ aggregation was shown to be dependent on its concentration (Figure S3d). Distinct from Co(II)(TMC), the modulating activity of the TMC ligand or Co(II)(EDTA) toward Aβ aggregation was not indicated (Figures 3b and S4c). In the case of the Co(II) salt, $Co(NO_3)_2$, the aggregation pathways of Aβ were influenced showing a different MW distribution from that triggered by Co(II)(TMC) (Figure S4c). Note that the interaction of the cobalt ion with Aβ could influence peptide aggregation pathways, similar to other metal ions, as previously reported.[1–5,7–9]

The aptitude of Co(II)(TMC) to inhibit Aβ_{42} aggregation appeared to be diminished compared to Aβ_{40}. A slight difference in the MW distribution of Aβ_{42} species was noticeable after 4, 8, and 24 h (Figure 3b, bottom). Ni(II)(TMC) and Zn(II)(TMC) also seemed to slightly alter the MW distribution of Aβ_{42} at the 24 h time point in the gel/Western blot, but TEM images revealed mostly dense clusters composed of long, thin fibrils, similar to those observed in the samples containing Aβ_{42} only and Aβ_{42} treated with the ligand (TMC) or Cu(II)(TMC) (Figure 3b,c). TEM samples of Aβ_{40} and Aβ_{42} treated with Co(II)(TMC), however, showed a distinct transformation into a distribution of more disperse

DOI: 10.1021/jacs.6b09681
J. Am. Chem. Soc. 2017, 139, 2234–2244

shorter, thinner, and needle-like species or amorphous aggregates (see the inset TEM image) (Figures 3c and S6). In addition to gel/Western and TEM, the influence of M(II)(TMC) complexes on formation of Aβ aggregates in inhibition experiments (Figure 3) was analyzed by turbidity and dynamic light scattering (DLS) measurements. As shown in Figure S6b (turbidity results), the amount of Aβ aggregates was noticeably diminished upon incubation with Co(II)(TMC) (by ca. 5-fold or higher) compared to the other M(II)(TMC) complexes. Additionally, the supernatant of the Co(II)(TMC)-treated Aβ sample, prepared after centrifugation (13,500 *g* for 30 min at 4 °C), was indicated to contain less Aβ aggregates (by ca. 1.5−60-fold) than those of the other complexes. Moreover, DLS results obtained from the supernatants of M(II)(TMC)-treated Aβ samples suggest that Co(II)(TMC), relative to the other M(II)(TMC), might induce Aβ aggregation toward a distribution of smaller sized particles (Figure S6c−e). Taken together, Co(II)(TMC) is identified to more significantly modulate Aβ aggregate formation than the other M(II)(TMC) complexes.

Similar trends were also displayed in disaggregation experiments (Figures S5 and S7). Only Co(II)(TMC) could reverse the assembly of preformed $A\beta_{40}$ and $A\beta_{42}$ aggregates. The reactivity with $A\beta_{40}$ also appeared to be correlated to the incubation period with no significant bands detected until 8 and 24 h (Figure S5b, top). Homologous to the $A\beta_{40}$ conditions, the extent to which Co(II)(TMC) was able to disaggregate preformed $A\beta_{42}$ aggregates also varied with the length of incubation; however, unlike $A\beta_{40}$, the most significant change in the MW distribution was discernible after 4 h (Figure S5b, bottom). The dissimilarity may be attributed to the increased $A\beta_{42}$ aggregation propensity, relative to that of $A\beta_{40}$.[1−5,7] Treatment of Co(II)(TMC) also perturbed the morphologies of $A\beta_{40}$ and $A\beta_{42}$ aggregates from the dense deposits of long fibrils that were detected in the complex-untreated Aβ controls to much less dense clusters of short, thin, and needle-like species similar to those in the inhibition experiments (Figures S5c and S7). Overall, our gel/Western blot and TEM investigations indicate that only Co(II)(TMC) is capable of significantly modulating the aggregation pathways of $A\beta_{40}$ and $A\beta_{42}$, which might be partially associated with its hydrolytic cleavage capability, while Ni(II)(TMC), Cu(II)(TMC), and Zn(II)(TMC) do not to an appreciable extent, despite the relatively high affinity binding sites in Aβ for Cu(II) and Zn(II) (i.e., $K_d \approx 10^{-9}$ and 10^{-6} M, respectively).[1−5,7]

Mechanistic Studies. *Adduct Formation of M(II)(TMC) Complexes with Aβ.* Electrospray ionization mass spectrometry (ESI-MS) and ion mobility mass spectrometry (IM-MS) were employed to determine whether the anti-amyloidogenic activity of Co(II)(TMC) was also partially a result of its ability to coordinate to Aβ and generate structurally altered Aβ−Co(II)(TMC) conformers, similar to the mode of action reported for Co(III) Schiff base complexes.[13] As shown in Figure S8, the peaks consistent with $A\beta_{40}$ bound to all four metal complexes [e.g., $A\beta_{40}$ + M(II)(TMC)] were detected. The Co(II)(TMC) spectrum, however, did have a unique peak at 1652.40 *m*/*z* that was assigned to $A\beta_{40}$ bound to two equivalents of Co(II)(TMC) [i.e., $A\beta_{40}$ + 2Co(II)(TMC)] (Figure S8). Additionally, the spectra of Cu(II)(TMC) and Zn(II)(TMC) also had two distinctive signals at 1575.83 and 1576.86 *m*/*z*, respectively. These peaks, absent in those of Co(II)(TMC) and Ni(II)(TMC), corresponded to the addition of a water molecule and a labile metal ion (Cu(II) and Zn(II), respectively) to $A\beta_{40}$ [i.e., $A\beta_{40}$ + M(II) + M(II)(TMC) + H_2O]. These data suggest that a small amount of Cu(II) and Zn(II) may be removed from TMC possibly by chelating to the N-terminal Cu(II) and Zn(II) binding sites (e.g., His6, His13, and His14) in Aβ.[1−5,7−9] The partial metal ion removal from Cu(II)(TMC) and Zn(II)(TMC) may explain why they did not significantly modulate the aggregation pathways of Aβ. Aβ fragments similar to those shown in the MALDI-MS studies were also distinguished, further supporting hydrolytic cleavage as the mode of action of Co(II)(TMC) (Figure S9 and Table S4). When compared to the $A\beta_{40}$ control, the Aβ/M(II)(TMC) adducts had a slightly longer drift time by IM-MS, indicative of more expanded structures, but there was no noticeable difference between Co(II)(TMC) and the other metal complexes (Figure S10). Collectively, our MS/IM-MS investigations suggest that the hydrolytic Aβ cleavage ability of Co(II)(TMC), along with its interaction with the peptide, might lead to modulate Aβ aggregation.

Isomerization of M(II)(TMC) Complexes. The ability of M(II)(TMC) complexes to form Aβ adducts was unexpected given the steric constraints associated with the *trans*-I conformation (Figure 1).[27,28] Isomerization of the *trans*-I complexes to the less sterically strained *trans*-III isomer which has two open coordination sites that can facilitate Aβ binding to form octahedral complexes may explain the Aβ−M(II)(TMC) adduct formations observed in our MS investigations (Figure 1). Additionally, the noticeable anti-amyloidogenic activity of Co(II)(TMC) may also be elucidated if this complex is able to undergo more facile isomerization, relative to the other M(II)(TMC) complexes. Moore and co-workers have shown that *trans*-I-M(II)(TMC) isomerization to *trans*-III-M(II)-(TMC) is highly dependent on solution conditions.[29] Thus, we monitored the UV−vis spectra of M(II)(TMC) under similar conditions as our *in vitro* studies to verify if *trans*-III-M(II)(TMC) can be formed. The peaks at ca. 479, 550, and 730 nm [for Co(II)(TMC)]; ca. 394, 510, and 658 nm [for Ni(II)(TMC)]; and ca. 615 nm [for Cu(II)(TMC)] were consistent with previous literature reports of the *trans*-I complexes (Figure S11).[28,30,33] With the exception of Ni(II)-(TMC), only slight increases in the absorbance of the *trans*-I-M(II)(TMC) complexes over the course of the experiment were observed and there was no indication of any λ_{max} blue shifts that would be suggestive of the generation of octahedral *trans*-III complexes (Figure S11).[28−31] Therefore, our optical studies suggest that no isomerization occurs under our *in vitro* conditions, and the possibility of Aβ coordinated to M(II)-(TMC) via a bis-His coordination mode is unlikely.

X-ray Structural Characterization of M(II)(TMC). The structural data of [Co(TMC)(NO_3)](NO_3) and [Ni(TMC)-(CH_3CN)](NO_3)$_2$ were obtained (Figure 1b,c) and used to compare the structures of Co(II)(TMC) and Ni(II)(TMC) nitrate complexes to each other and to the previously reported Cu(II)(TMC) and Zn(II)(TMC) perchlorate complexes.[31,41,42] The degree of distortion in M(II)(TMC) complexes is highly dependent on the identity of the ligand occupying the open coordination site. For this reason, comparison to calculations with identical ligands at the fifth coordination site was also conducted (vide infra).

As shown in Figure 1, both Co(II)(TMC) and Ni(II)(TMC) complexes were in the expected *trans*-I conformation. A nitrate molecule was observed to be bound to the *syn* face of Co(II)(TMC) in an unusual bidentate fashion forming a distorted six-coordinate complex.[43] The asymmetric unit of

DOI: 10.1021/jacs.6b09681
J. Am. Chem. Soc. 2017, 139, 2234−2244

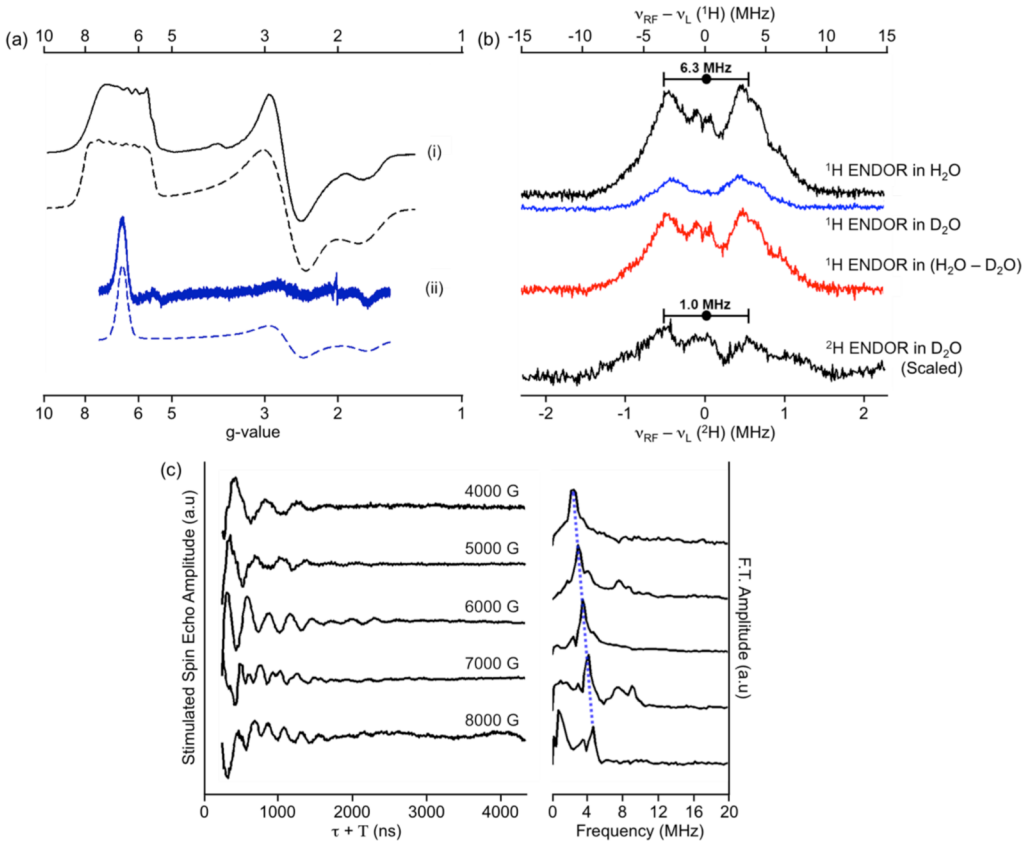

Figure 4. EPR measurements of Co(II)(TMC). (a) (i) X-band CW-EPR spectrum of Co(II)(TMC) (solid black) and its simulated spectrum (dashed black); (ii) W-band Electron Spin Echo-detected EPR spectrum (solid blue) of Co(II)(TMC) and its simulated spectrum (dashed blue). The following parameters were used in the simulation: g = [2.42, 2.42, 2.21], A_{Co} = [0, 60, 0] G, $D \geq 13$ cm^{-1}, E/D = 0.3 (b) ^{1}H Davies ENDOR spectra of Co(II)(TMC) in H_2O (black) and in D_2O (blue).The subtracted ^{1}H ENDOR spectrum is shown in red. ^{2}H Mims ENDOR in D_2O (black). (c) Q-band three-pulse time-domain (left) and the frequency domain (right) ESEEM spectra of Co(II)(TMC). The blue dashed line in the frequency domain indicates the ^{17}O Larmor frequency at each field. The detailed experimental conditions are described in the Supporting Information [the EPR samples were prepared in H_2O:glycerol (7:3, v/v)].

Ni(II)(TMC) contained two complexes, each with an CH_3CN ligand at the axial site, but with one being slightly more distorted than the typically perfect square pyramidal complexes previously reported (Figure 1c and Table S3).[44−46] In addition, Co(II) was positioned the farthest above the macrocyclic plan (i.e., 0.532 Å) compared to ca. 0.221 Å for Ni(II)(TMC), 0.303 Å for Cu(II)(TMC), and 0.484 Å for Zn(II)-(TMC).[31,41,42,44−48] Furthermore, DFT-predicted structures of the water-bound ground-state M(II)(TMC) complexes (i.e., $[M(TMC)(H_2O)]^{2+}$) also presented a noticeable distortion in the structure of Co(II)(TMC); however, Zn(II)(TMC) also had comparable dihedral angles and distances of its metal center sitting above the macrocyclic plane (Table S5). More facile substrate entry (e.g., Aβ) to the metal center may be facilitated by such distortion and the metal ion sitting farther above the macrocyclic plane because it reduces the adverse steric effects associated with all four methyl groups located on the same side of the macrocyclic plane where the axial ligands coordinate (Figure 1b,c).[23,27,28,30−33,41,42,44−50] Overall, X-ray crystallographic and DFT-optimized structures may help to explain why Co(II)(TMC), showing a more distorted conformation, exhibits enhanced reactivities with peptides relative to the other complexes (vide infra).

EPR Studies of Co(II)(TMC). In order to characterize the structure of Co(II)(TMC) in solution, continuous-wave and pulsed multifrequency EPR techniques were employed. The X-band CW-EPR spectrum of Co(II)(TMC) exhibits a rhombic spectrum with the g tensor, g_{eff} = [6.3, 2.7, 1.7] which arises from high-spin, Co(II)(S = 3/2) (Figure 4a (i)). The hyperfine coupling from ^{59}Co (100%, I = 7/2) was observed around $g \approx 6$. In addition, the W-band (94 GHz) EPR data display a rhombic signal similar to the X-band EPR spectrum; however, the hyperfine splitting from ^{59}Co cannot be observed (Figure 4a (ii)). To obtain more accurate spin Hamiltonian parameters, simulations of the X-band and W-band CW-EPR experiments were carried out simultaneously (Figure 4a, dashed lines). The zero-field splitting parameter, D, of high-spin Co(II) is supposed to be large, hence being insensitive in an X-band experiment; however, it becomes more sensitive when simulating the W-band EPR spectrum. The spin Hamiltonian parameters obtained from the simulations are similar to those that have a five-coordinate species.[51,52] In particular, a E/D of ca. 0.3 indicates that the complex has a distorted coordination geometry.[51−53] Thus, the CW-EPR data indicate that Co(II)-(TMC) has a distorted five-coordinate geometry, consistent with the UV−vis and DFT results (vide infra).

To examine if water is bound to Co(II)(TMC), we conducted the ^{1}H as well as ^{2}H ENDOR experiments (Figures 4b and S13). The ^{1}H ENDOR spectrum exhibits doublets centered at the Larmor frequency of a proton and separated by its hyperfine coupling, A: $\nu\pm = \nu_H \pm A/2$. The ENDOR intensity of the hyperfine coupling of $A \approx 6.3$ MHz signal in the

DOI: 10.1021/jacs.6b09681
J. Am. Chem. Soc. 2017, 139, 2234−2244

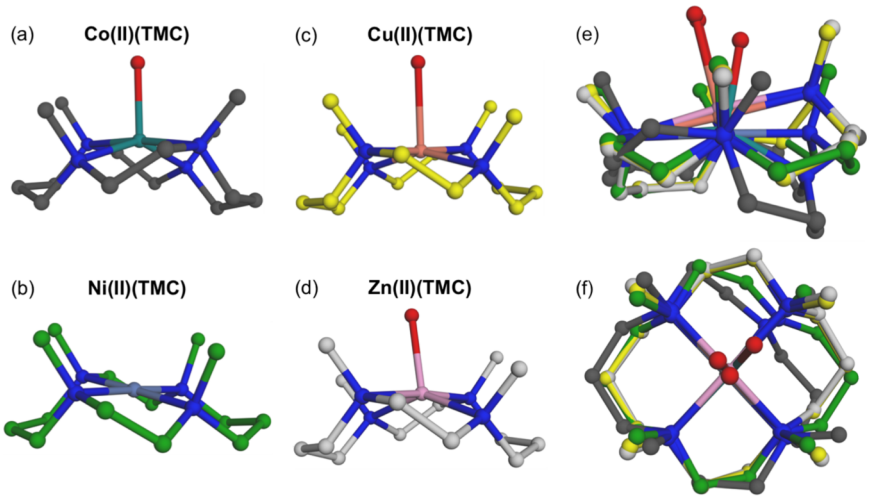

Figure 5. Computational examination of M(II)(TMC) complexes. Calculated structures of (a) $[Co(TMC)(H_2O)]^{2+}$, (b) $[Ni(TMC)]^{2+}$, (c) $[Cu(TMC)(H_2O)]^{2+}$, and (d) $[Zn(TMC)(H_2O)]^{2+}$. (e,f) Overlay of the ground-state M(II)(TMC) structures presented from the side and top.

^{1}H ENDOR spectrum prepared in D_2O is decreased significantly. In addition, the ^{2}H ENDOR spectrum exhibits the doublet centered at the ^{2}H Larmor frequency and is split by ca. 1.0 MHz. The magnitude of the hyperfine coupling (1.0 MHz) is comparable to the proton hyperfine coupling of 6.3 MHz if scaled by the magnetogyric ratio of $\gamma(^1H/^2H)$. Thus, ^{1}H and ^{2}H ENDOR spectra indicate that there is an exchangeable proton(s). To verify if the exchangeable proton originates from water bound to Co(II), the ^{1}H ENDOR experiment on $CoCl_2$ was performed in H_2O. Figure S15 presents that the largest hyperfine coupling of a proton is ca. 6.4 MHz at $g \approx 3.5$. The magnitude of the hyperfine coupling of ^{1}H is comparable to the one we observed in Co(II)(TMC). Taken together, these results support that the ^{1}H ENDOR signal observed in the Co(II)(TMC) spectrum arises from the ^{1}H-bound water to the cobalt center.

Moreover, we have also performed the ^{17}O ESEEM experiment on the Co(II)(TMC) sample prepared in ^{17}O-labeled water. Figure 4c displays the time-domain and the frequency-domain three-pulse ESEEM spectra, respectively. The time-domain spectra (Figure 4c, left) displayed the ratio of $^{17}O/^{16}O$ to eliminate contributions from other nuclei and also τ, the time between the first and the second pulse, was chosen to maximize the modulation of the ^{17}O nuclei. The time-domain ESEEM data exhibit the modulation arising from ^{17}O, and the Fourier-transformed frequency domain further confirms that ^{17}O is coupled to Co(II) by showing the ^{17}O peak around the Larmor frequency of the ^{17}O nucleus. To validate the magnitude of the hyperfine coupling of ^{17}O ligated to the Co(II) center, the ^{17}O ESEEM experiments on $CoCl_2 \cdot 6H_2O$ prepared in ^{17}O-labeled water (70% enrichment) were performed (Figure S16). The ^{17}O three-pulse ESEEM spectrum of $CoCl_2$ shows the similar field-dependent ^{17}O modulation pattern as seen for Co(II)(TMC) prepared in $H_2{}^{17}O$, which indicates that the ^{17}O signal arises from the water coordinated to the metal ion (Figure S16). Overall, our EPR results indicate that water is the ligand bound to the distorted pentacoordinated (possibly, TBP) Co(II)(TMC) complex in solution, implying the water activation by Co(II)(TMC) as the hydrolytic mechanism (vide infra).

Computational Investigations. a. Characterization of M(II)(TMC) Complexes in Aqueous Solutions. Regarding a possible mechanism by which the hydrolysis of Aβ's amide bonds is facilitated by the Co(II)(TMC) complex, it needs to be assessed whether a water molecule can be activated to a hydroxide ion by the Co(II)(TMC) complex (vide infra, Figure 7b). To assess the axial ligand of the M(II)(TMC) complexes in aqueous solutions, DFT and time-dependent DFT (TDDFT) calculations were performed for their water- and hydroxo-ligated forms in all possible spin states. To ensure the reliability of the computational analyses, a proper combination of functional and basis set was selected (Figures S17 and S18), reproducing the quartet ground state, determined by EPR, and the water ligation, determined by UV−vis, of the Co(II)(TMC) complex (Figures 4 and S19). Free energies calculated from the validated DFT method suggest that in aqueous solutions, all M(II)(TMC) complexes have a water molecule as an axial ligand rather than a hydroxide ligand, except for Ni(II)(TMC) which stays four-coordinated without having an axial ligand in its ground singlet state (Table S6). Specifically, the UV−vis feature of the Co(II)(TMC) complex is best matched with the ligand-field (LF) transitions calculated from the water-coordinated Co ($S = 3/2$) and Cu ($S = 1/2$) complexes and the four-coordinate Ni ($S = 0$) complex (Figures 5 and S20).

b. Activation of a Water Molecule by M(II)(TMC) Complexes for Amide Hydrolysis. The above spectroscopic and DFT analyses show that, in aqueous solutions, water binds to the metal centers of Co(II)(TMC), Cu(II)(TMC), and Zn(II)(TMC), not as a hydroxide ion but as a water molecule. Thus, the energies required to deprotonate these ground-state complexes were calculated (Table S6a). The pK_a value of the ground-state $[Co(TMC)(H_2O)]^{2+}$ is calculated to be 8.4 which is consistent with the experimental value of 8.5 obtained through UV−vis variable-pH titration experiments (Figure S19).[54] Given the range of typical pK_a values of amino acids (4−12.5) and their possible variations depending on micro-environment, the pK_a value of ca. 8.5 suggests that $[Co(TMC)(H_2O)]^{2+}$ would have a chance to be deprotonated by nearby amino acids thus generating a hydroxide ion (Table S7). In contrast, this deprotonation of a water ligand appears to be less plausible for the other complexes. The pK_a values of the $[Cu(TMC)(H_2O)]^{2+}$ and $[Zn(TMC)(H_2O)]^{2+}$ complexes, which could not be determined experimentally due to the absence of proper pH-sensitive absorption features, are

DOI: 10.1021/jacs.6b09681
J. Am. Chem. Soc. 2017, 139, 2234−2244

calculated to be 17.8 and 12.0, respectively. These pK_a values are inaccessibly high in physiological conditions, implying that the $[Cu(TMC)(H_2O)]^{2+}$ and $[Zn(TMC)(H_2O)]^{2+}$ complexes would not be activated to the hydroxide-coordinated species. Despite the fact that the ground-state Ni(II)(TMC) complex is calculated to be four-coordinate, the Ni(II) center can be converted to a high-spin state with a hydroxide ligand; the pK_a for the reaction of $[Ni(TMC)]^{2+}$ (S = 0) + $2H_2O$ → $[Ni(TMC)(OH)]^{+}$ (S = 1) + H_3O^{+} is known to be 10.1 and thus accessible (Figure S19).[30]

c. Activation of an Amide Bond by M(II)(TMC) Complexes. One other way of promoting amide hydrolysis is to activate the amide bond by having the carbonyl oxygen of the amide bond bound to the metal center and thus generating a more electrophilic character (see Figure 7b, below). To assess this possibility, the energies required to replace the water ligand of the ground-state M(II)(TMC) complexes with the amide carbonyl oxygen were calculated (Table S6b). Except for Ni(II)(TMC) which does not bind to the amide in the singlet ground state, the water ligand could be replaced with a less than 6 kcal/mol free energy. Considering that peptide hydrolysis is downhill by 2−4 kcal/mol,[55] amide activation via its carbonyl ligation to the metal center seems to be thermodynamically feasible driven by the exergonic peptide hydrolysis (although this does not necessarily suggest fast kinetics). The possibility of having both water and amide ligands on the same metal center was discarded based on its excessive high energy calculated relative to the ground state (see Figure 7b (iv)). Combining the two plausible activation pathways discussed above, the binuclear mechanism in Figure 7b (v) can be conclusively suggested for $[Co(TMC)(H_2O)]^{2+}$. Particularly, in the ground state, while other complexes have square pyramidal (or square planar) structures, only the cobalt complex has a TBP structure (Figure 7b) which would allow the TMC ligand to be distorted and the open coordination site to be less sterically hindered and thus more easily accommodate substrate entry and possible binuclear interactions, as shown in Figure 5e,f.

Biological Applicability of M(II)(TMC) Complexes. To gauge the practicality of Co(II)(TMC) as an anti-amyloidogenic agent, we first assessed its potential blood−brain barrier (BBB) permeability by the parallel artificial membrane permeability assay adapted for the BBB (PAMPA-BBB; Table S8). Co(II)(TMC) was predicted to passively diffuse across the BBB based on its −log P_e value (5.0 ± 0.2) compared to those of other previously reported BBB-permeable molecules.[56,57] Next, the MTT assay was employed to evaluate the toxicity of Co(II)(TMC) and its regulatory ability toward Aβ-induced toxicity using human neuroblastoma SH-SY5Y (5Y) cells. Co(II)(TMC) was determined to have relatively low toxicity with an IC_{50} of 286 ± 13 μM (Figure S21). In addition, the toxicity of Aβ_{40} and Aβ_{42} incubated with M(II)(TMC) or the Co(II) salt (i.e., $Co(NO_3)_2$) was determined in living cells. Both Aβ_{40} and Aβ_{42} pretreated with Co(II)(TMC) for 8 and 24 h were indicated to be less toxic in living cells compared to complex-untreated peptides (Figure 6; preincubation for 8 and 24 h). In addition, Co(II)(TMC) was capable of recovering Aβ-induced cellular toxicity without preincubation (Figure 6; preincubation for 0 h). Such the regulatory activity of Co(II)(TMC) toward Aβ with and without preincubation was more noticeable than that of the other M(II)(TMC) complexes and the Co(II) salt (Figure S22). Based on our cytotoxicity studies, we suggest that (i) the cellular tolerance for Co(II)(TMC) may be due to its preferential cleavage of Aβ which lacks a well-defined tertiary (or quaternary) structure over essential biological proteins that are highly folded (the hypothesis, vide infra); (ii) toxicity triggered by Aβ could be controlled by modulation of peptide aggregation via hydrolytic cleavage, along with the interaction with the peptide (e.g., complex formation).

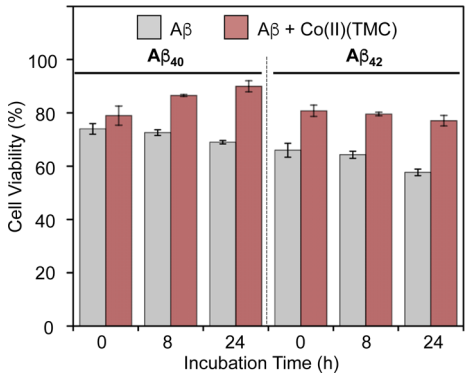

Figure 6. Cell viability of Aβ_{40} or Aβ_{42} incubated with Co(II)(TMC). Aβ peptides pretreated with or without Co(II)(TMC) for 0, 8, and 24 h were incubated with SH-SY5Y cells for 24 h at 37 °C. Cell viability was determined by the MTT assay. Values of cell viability (%) were calculated compared to those of cells treated with equivalent amounts of water only (0−10%, v/v). Conditions (final concentrations): [Aβ_{40} or Aβ_{42}] = 40 μM; [Co(II)(TMC)] = 40 μM. Error bars represent the standard error from three independent experiments (P < 0.05).

In order to test the hypothesis that due to the disordered structure, the amide bonds in Aβ may be more accessible to Co(II)(TMC) for hydrolysis with respect to the amide bonds in tightly folded proteins which may be more protected from undesired cleavage, we analyzed Co(II)(TMC)-treated ubiquitin samples spiked with an internal standard (i.e., melittin) for monomer suppression and peptide fragmentation by MALDI-MS (Figure S23). Ubiquitin was chosen for its similarity in size to Aβ and its well-defined and tightly folded structure.[58] Unlike the Aβ_{40} samples incubated with Co(II)(TMC), the ubiquitin samples did not produce any detectable fragments and there was no noticeable reduction in the singly charged monomer peak. Additionally, Co(II)(TMC) also appeared to maintain its activity in the presence of biologically relevant reducing agents such as glutathione (GSH) (Figure S24). Together, these studies show that Co(II)(TMC) is BBB permeable and relatively low in cytotoxicity with preferential cleavage activity toward amyloidogenic peptides over highly structured proteins, along with regulatory activity against Aβ-related cytotoxicity, which suggests its potential use for further biological applications.

■ DISCUSSION

The proteolytic and anti-amyloidogenic reactivities of M(II)(TMC) complexes (M = Co, Ni, Cu, and Zn) with Aβ were investigated indicating that Co(II)(TMC) was identified to more noticeably cleave Aβ peptides and control their aggregation than the other M(II)(TMC) complexes. Based on the biochemical, spectroscopic, mass spectrometric, and computational studies reported herein, we were able to conceive of two main pathways that may explain the anti-amyloidogenic activity of Co(II)(TMC). The first possible pathway (Figure 7a) is the binding of Co(II)(TMC) to Aβ that in turn would facilitate conformational changes in Aβ and thus

DOI: 10.1021/jacs.6b09681
J. Am. Chem. Soc. 2017, 139, 2234−2244

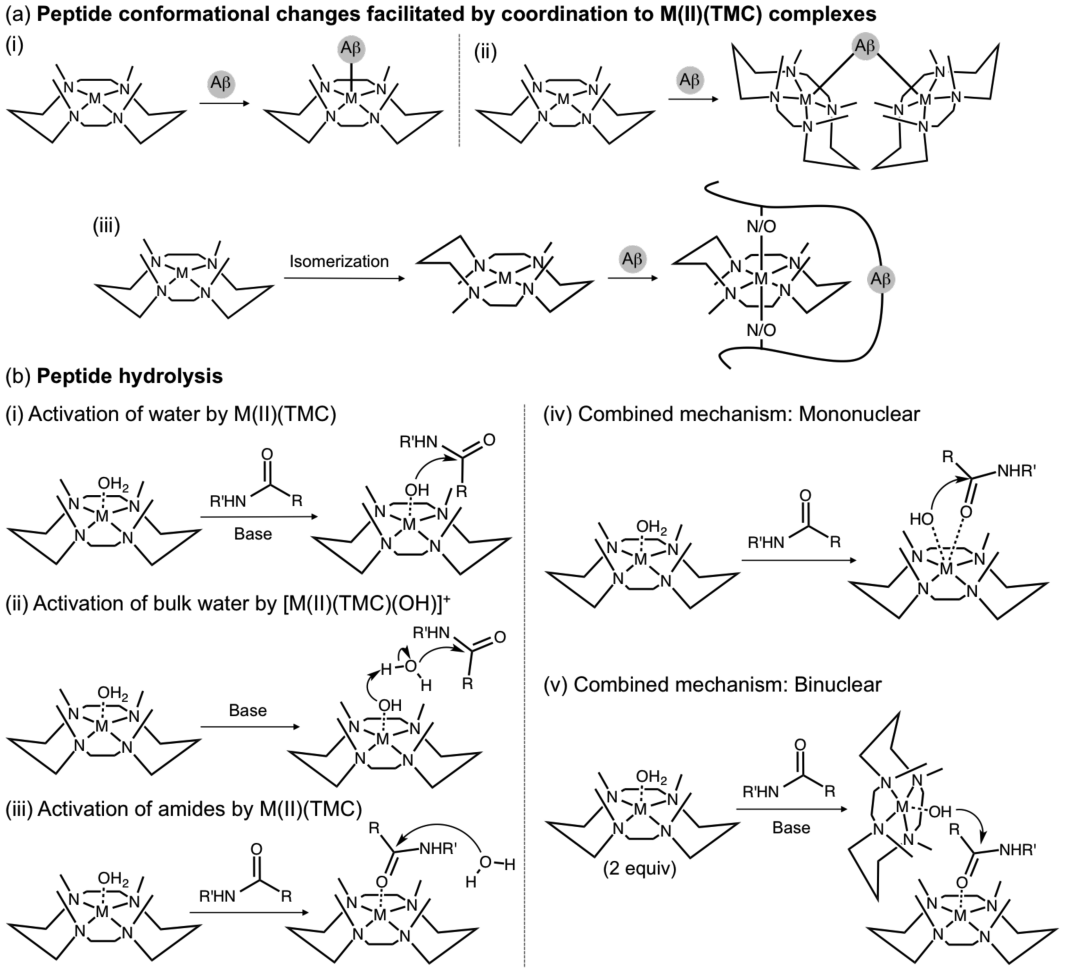

Figure 7. Schemes of the potential modes of action of M(II)(TMC) to modulate Aβ aggregation. (a) The conformation of Aβ is altered leading to the generation of off-pathway aggregates through (i) coordination to the metal center of M(II)(TMC) [e.g., Aβ–M(II)(TMC)]; (ii) intermolecular coordination of Aβ to two equivalents of M(II)(TMC); (iii) isomerization to the *trans*-III stereoisomer and subsequent formation of an octahedral complex. (b) Metal complexes facilitate the hydrolysis of amide bonds to generate Aβ fragments. Amide bond hydrolysis can be catalyzed by (i) the activation of water by M(II)(TMC) to generate metal–hydroxo nucleophiles; (ii) the activation of bulk water by [M(II)(TMC) (OH)]$^+$ to form hydroxide nucleophiles; (iii) Lewis acid activation of the amide bonds; (iv) a mononuclear combined mechanisms where both substrates (i.e., water and amide) are coordinated to the metal complex; (v) a binuclear combined mechanism where two equivalents of M(II)(TMC) are used to produce the hydroxide source and activate the amide bond.

prohibit the formation of toxic aggregates. Such a trans-formation in peptide conformation could be envisioned to occur via multiple mechanisms (Figure 7a, (i)–(iii)). The generation of intramolecular protein–M(II)(TMC) complexes (Figure 7a (iii)) can be reasonably eliminated as a possible mechanism due to the absence of optical changes in the spectra of Co(II)(TMC), Ni(II)(TMC), and Cu(II)(TMC) that would be consistent with the formation of *trans*-III octahedral complexes. MS studies detected peaks consistent with the formation of Aβ–Co(II)(TMC) adducts and IM studies showed a slight increase in the drift time of samples treated with Co(II)(TMC), indicative of a slightly expanded Aβ conformation. Combined, these studies suggest that while the complex formation with Aβ showing the slight change in peptide conformation may contribute to Co(II)(TMC)'s modulating reactivity toward Aβ aggregation, it does not alone provide a mechanistic explanation for why only Co(II)(TMC) alters Aβ aggregation.

Hydrolytic cleavage of Aβ's amide bonds by Co(II)(TMC) may be an alternate route through which it is able to inhibit the formation of fibrils and disassemble mature aggregates into smaller and amorphous species. As shown in Figure 7b, the hydrolysis of amide bonds may proceed via three main pathways. First, hydroxide nucleophiles could be produced by the activation and deprotonation of water molecules by M(II)(TMC) to generate metal–hydroxo species (i.e., [M-(TMC) (OH)]$^+$) that can attack the carbonyl and subsequently hydrolyze the amide bonds (Figure 7b (i)). Additionally, the metal–hydroxo species could also activate bulk water molecule, causing a local increase in the concentration of hydroxide nucleophiles near the peptide bonds (Figure 7b (ii)). Such mechanisms would require the relatively facile deprotonation of the ground-state [M(TMC)(H_2O)]$^{2+}$. Based on our pH-dependent spectroscopic titrations and TDDFT calculations, Co(II)(TMC) would be expected to be the most reactive of the M(II)(TMC) complexes through this mechanistic pathway, thus explaining our observations from the gel/Western blot, TEM, turbidity, and DLS studies. The deprotonation of the ground-state [M(TMC)(H_2O)]$^{2+}$ complexes by nearby amino acids was found to be most plausible for the Co(II)(TMC) complex (pK_a of 8.5 for Co(II)(TMC) versus 10.1–17.8 for the other M(II)(TMC) complexes). In fact, EPR studies validated

DOI: 10.1021/jacs.6b09681
J. Am. Chem. Soc. 2017, 139, 2234–2244

the existence of a distorted five-coordinate Co(II)(TMC) with exchangeable protons on the water molecule occupying the open coordination site. Ni(II)(TMC), Cu(II)(TMC), and Zn(II)(TMC), found to have pK_a values greater than 10, would be expected to have negligible amounts of metal−hydroxo species generated under physiological conditions thus explaining their lower proteolytic activity. Furthermore, a mechanism of water activation would also explain the enhanced Aβ_{40} monomer signal suppression and fragmentation detected in the Co(II)(TMC)-treated MALDI-MS samples incubated at a slightly basic pH (e.g., pH 8.5).

A second mechanism through which amide bonds could be hydrolyzed involves the ligand exchange of the water molecule of the ground-state complexes with an amide from the backbone of Aβ. Binding of the carbonyl oxygen atom to the metal center can prime the amide for nucleophilic attack by generating a more electrophilic substrate (Figure 7b (iii)). Computationally, ligand exchange was found to be energetically feasible for M(II)(TMC) especially when one considers the overall exergonic process of peptide hydrolysis (2−4 kcal/mol downhill) (Table S6); however, this mechanism alone does not seem to explain the enhanced reactivity of Co(II)(TMC).

Given the respective feasibility of both pathways, it also seems plausible that a combined mechanism could occur where the metal complexes could simultaneously generate metal−hydroxo nucleophiles as well as activate Aβ's amide bonds (Figure 7b (iv) and (v)). Theoretically, a combined mechanism may occur via a mononuclear (Figure 7b (iv)) or binuclear (Figure 7b (v)) pathway. The intramolecular mechanism with both water and amide ligands bound to the metal center was excluded due to its relatively high calculated energy. An intermolecular system where one metal complex generates a hydroxide source and another equivalent complex activates the amide does not seem unreasonable given the plausibility of the two independent pathways. Based on our results on the concentration-dependent proteolytic activity of Co(II)(TMC) toward Aβ (Figure S3), a binuclear pathway for such the hydrolytic cleavage reaction might be possible. Overall, our studies suggest the activation of water by Co(II)(TMC) to be the likely mechanism of hydrolysis; however, the extent or degree to which they may also activate the amide or participate in a binuclear mode of action is still not completely clear. Moving forward, these mechanistic insights also suggest that hydrolytic cleavage may be further improved by redirecting the mechanism toward the concerted process. Studies are currently underway to test this hypothesis.

CONCLUSION

To explore metal-mediated Aβ hydrolysis and obtain the anti-amyloidogenic activity of metal complexes, we developed a series of divalent metal tetra-*N*-methylated cyclam complexes with the purpose of achieving a degree of tunability and control through their unique stereochemistry and coordination spheres which do not exist in the previously reported octahedral Co(III)(cyclen) complexes.[19] To our surprise, Co(II)(TMC) is demonstrated to more significantly cleave both Aβ_{40} and Aβ_{42} and modulate Aβ aggregation, compared to the other M(II)(TMC) complexes. MS and IM-MS studies attributed that the metal center directed proteolytic and anti-amyloidogenic activities of M(II)(TMC) complexes with Aβ via promotion of amide bond hydrolysis as well as the interaction with Aβ (e.g., complex formation[59−61]).

Spectroscopic and computational studies identified the activation of water by M(II)(TMC) as the most reasonable pathway that would explain the enhanced proteolytic activity of Co(II)(TMC) with respect to the other complexes due to its relatively acidic pK_a of the water-bound ground-state complex, but the activation of amide bonds by Co(II)(TMC) or a combined binuclear mechanism could not be ruled out. Furthermore, the biological applicability of Co(II)(TMC) was established by maintaining its proteolytic activity toward Aβ under biologically relevant conditions as well as showing its ability to diffuse across the BBB, relatively low cytotoxicity which appears to be partially a result of its preferential interaction with amyloidogenic proteins over structured substrates, and regulatory activity against toxicity induced by Aβ peptides. Taken together, our findings on the metal center dependence for amyloidogenic peptide cleavage, along with the mechanistic insights, not only bestow a novel strategy through which the cleavage activity and selectivity of proteolytic metal complexes can be tuned, but it also shows that high cleavage propensity, which often leads to poor substrate selectivity, is not required to achieve the desired anti-amyloidogenic reactivity.

ASSOCIATED CONTENT

Supporting Information

The Supporting Information is available free of charge on the ACS Publications website at DOI: 10.1021/jacs.6b09681.

Experimental section, Tables S1−S8, and Figures S1−S24 (PDF)

X-ray crystallographic data for [Co(TMC)(NO_3)](NO_3) (CIF)

X-ray crystallographic data for [Ni(TMC)(CH_3CN)]-(NO_3)$_2$ (CIF)

AUTHOR INFORMATION

Corresponding Authors

*mhlim@unist.ac.kr

*jaeheung@dgist.ac.kr

*kiyoung.park@kaist.ac.kr

*shkim7@kbsi.re.kr

ORCID

Sun Hee Kim: 0000-0001-6557-1996

Mi Hee Lim: 0000-0003-3377-4996

Notes

The authors declare no competing financial interest.

ACKNOWLEDGMENTS

This work was supported by National Research Foundation of Korea (NRF) grants funded by the Korean government [NRF-2014R1A2A2A01004877 and 2016R1A5A1009405 (to M.H.L.); 2014R1A1A2056051 (to J.C.); 2015R1C1A1A-02036917 (to K.P.)]; the 2017 Research Fund (Project Number 1.170014.01) of UNIST (to M.H.L.); the Ministry of Science, ICT and Future Planning [16-BD-0403, 2014-M1A8A1049320, and 2016M3D3A01913243 (to J.C.)]; the Ministry of Oceans and Fisheries (20150220) of Korea (to J.C.); the supercomputing resources (KSC-2015-C2-0002) of Korea Institute of Science and Technology Information (KISTI) (to K.P.); the C1 Gas Refinery Program through the NRF funded by the Ministry of Science, ICT and Future Planning [2015M3D3A1A01064876 (to S.H.K.) and 2015-

DOI: 10.1021/jacs.6b09681
J. Am. Chem. Soc. 2017, 139, 2234−2244

M3D3A1A01064889 (K.P.)]; and the National Research Council of Science and Technology through the Degree & Research Center Program (DRC-14-3-KBSI to S.H.K.). J.K. thanks the Global Ph.D. fellowship program for support through the National Research Foundation of Korea (NRF) funded by the Ministry of Education (NRF-2015HIA2A-1030823). We thank Dr. Hyuck Jin Lee for assistant with our DLS mesurements.

REFERENCES

(1) Derrick, J. S.; Lim, M. H. *ChemBioChem* **2015**, *16*, 887.
(2) Savelieff, M. G.; Lee, S.; Liu, Y.; Lim, M. H. *ACS Chem. Biol.* **2013**, *8*, 856.
(3) Savelieff, M. G.; DeToma, A. S.; Derrick, J. S.; Lim, M. H. *Acc. Chem. Res.* **2014**, *47*, 2475.
(4) Jakob-Roetne, R.; Jacobsen, H. *Angew. Chem., Int. Ed.* **2009**, *48*, 3030.
(5) Kepp, K. P. *Chem. Rev.* **2012**, *112*, 5193.
(6) Alzheimer's Association. *Alzheimer's Dementia* **2015**, *11*, 332.
(7) Rodríguez-Rodríguez, C.; Telpoukhovskaia, M.; Orvig, C. *Coord. Chem. Rev.* **2012**, *256*, 2308.
(8) Scott, L. E.; Orvig, C. *Chem. Rev.* **2009**, *109*, 4885.
(9) Hayne, D. J.; Lim, S.; Donnelly, P. S. *Chem. Soc. Rev.* **2014**, *43*, 6701.
(10) Valensin, D.; Gabbiani, C.; Messori, L. *Coord. Chem. Rev.* **2012**, *256*, 2357.
(11) Hureau, C.; Faller, P. *Dalton Trans.* **2014**, *43*, 4233.
(12) Collin, F.; Sasaki, I.; Eury, H.; Faller, P.; Hureau, C. *Chem. Commun.* **2013**, *49*, 2130.
(13) Heffern, M. C.; Velasco, P. T.; Matosziuk, L. M.; Coomes, J. L.; Karras, C.; Ratner, M. A.; Klein, W. L.; Eckermann, A. L.; Meade, T. J. *ChemBioChem* **2014**, *15*, 1584.
(14) Barnham, K. J.; Kenche, V. B.; Ciccotosto, G. D.; Smith, D. P.; Tew, D. J.; Liu, X.; Perez, K.; Cranston, G. A.; Johanssen, T. J.; Volitakis, I.; Bush, A. I.; Masters, C. L.; White, A. R.; Smith, J. P.; Cherny, R. A.; Cappai, R. *Proc. Natl. Acad. Sci. U. S. A.* **2008**, *105*, 6813.
(15) Kenche, V. B.; Hung, L. W.; Perez, K.; Volitakes, I.; Ciccotosto, G.; Kwok, J.; Critch, N.; Sherratt, N.; Cortes, M.; Lal, V.; Masters, C. L.; Murakami, K.; Cappai, R.; Adlard, P. A.; Barnham, K. J. *Angew. Chem., Int. Ed.* **2013**, *52*, 3374.
(16) Donnelly, P. S.; Caragounis, A.; Du, T.; Laughton, K. M.; Volitakis, I.; Cherny, R. A.; Sharples, R. A.; Hill, A. F.; Li, Q. X.; Masters, C. L.; Barnham, K. J.; White, A. R. *J. Biol. Chem.* **2008**, *283*, 4568.
(17) Kim, H. M.; Jang, B.; Cheon, Y. E.; Suh, M. P.; Suh, J. *J. Biol. Inorg. Chem.* **2009**, *14*, 151.
(18) Chei, W. S.; Ju, H.; Suh, J. *J. Biol. Inorg. Chem.* **2011**, *16*, 511.
(19) Suh, J.; Yoo, S. H.; Kim, M. G.; Jeong, K.; Ahn, J. Y.; Kim, M.-S.; Chae, P. S.; Lee, T. Y.; Lee, J.; Lee, J.; Jang, Y. A.; Ko, E. H. *Angew. Chem., Int. Ed.* **2007**, *46*, 7064.
(20) Jeon, J. W.; Son, S. J.; Yoo, C. E.; Hong, I. S.; Suh, J. *Bioorg. Med. Chem.* **2003**, *11*, 2901.
(21) Gonzalez, P.; da Costa, V. C. P.; Hyde, K.; Wu, Q.; Annunziata, O.; Rizo, J.; Akkaraju, G.; Green, K. N. *Metallomics* **2014**, *6*, 2072.
(22) Lanza, V.; D'Agata, R.; Iacono, G.; Bellia, F.; Spoto, G.; Vecchio, G. *J. Inorg. Biochem.* **2015**, *153*, 377.
(23) Liang, X.; Sadler, P. J. *Chem. Soc. Rev.* **2004**, *33*, 246.
(24) Wu, W.-H.; Lei, P.; Liu, Q.; Hu, J.; Gunn, A. P.; Chen, M.-S.; Rui, Y.-F.; Su, X.-Y.; Xie, Z.-P.; Zhao, Y.-F.; Bush, A. I.; Li, Y. M. *J. Biol. Chem.* **2008**, *283*, 31657.
(25) Yang, Y.; Chen, T.; Zhu, S.; Gu, X.; Jia, X.; Lu, Y.; Zhu, L. *Integr. Biol.* **2015**, *7*, 655.
(26) Chen, T.; Wang, X.; He, Y.; Zhang, C.; Wu, Z.; Liao, K.; Wang, J.; Guo, Z. *Inorg. Chem.* **2009**, *48*, 5801.
(27) Barefield, K. E. *Coord. Chem. Rev.* **2010**, *254*, 1607.
(28) Micheloni, M.; Paoletti, P.; Bürki, S.; Kaden, T. A. *Helv. Chim. Acta* **1982**, *65*, 587.
(29) Moore, P.; Sachinidis, J.; Willey, G. R. *J. Chem. Soc., Chem. Commun.* **1983**, 522.
(30) Herron, N.; Moore, P. *Inorg. Chim. Acta* **1979**, *36*, 89.
(31) Maimon, E.; Zilbermann, I.; Golub, G.; Ellern, A.; Shames, A. I.; Cohen, H.; Meyerstein, D. *Inorg. Chim. Acta* **2001**, *324*, 65.
(32) Crick, I. S.; Tregloan, P. A. *Inorg. Chim. Acta* **1988**, *142*, 291.
(33) Barefield, K. E.; Wagner, F. *Inorg. Chem.* **1973**, *12*, 2435.
(34) Terwilliger, T. C.; Eisenberg, D. *J. Biol. Chem.* **1982**, *257*, 6016.
(35) Chin, J. *Acc. Chem. Res.* **1991**, *24*, 145.
(36) Buckingham, D. A.; Harrowfield, J. M.; Sargeson, A. M. *J. Am. Chem. Soc.* **1974**, *96*, 1726.
(37) Buckingham, D. A.; Dekkers, J.; Sargeson, A. M.; Wein, M. *J. Am. Chem. Soc.* **1972**, *94*, 4032.
(38) Hettich, R.; Schneider, H.-J. *J. Am. Chem. Soc.* **1997**, *119*, 5638.
(39) Buckingham, D. A.; Keene, F. R.; Sargeson, A. M. *J. Am. Chem. Soc.* **1974**, *96*, 4981.
(40) Takasaki, B. K.; Kim, J. H.; Rubin, E.; Chin, J. *J. Am. Chem. Soc.* **1993**, *115*, 1157.
(41) Lu, T.-H.; Shui, W.-Z.; Tung, S.-F.; Chi, T.-Y.; Liao, F.-L.; Chung, C.-S. *Acta Crystallogr., Sect. C: Cryst. Struct. Commun.* **1998**, *54*, 1071.
(42) Panneerselvam, K.; Lu, T.-H.; Chi, T.-Y.; Tung, S.-F.; Chung, C.-S. *Anal. Sci.* **1999**, *15*, 205.
(43) Kumar, P.; Lee, Y.-M.; Hu, L.; Chen, J.; Park, Y. J.; Yao, J.; Chen, H.; Karlin, K. D.; Nam, W. *J. Am. Chem. Soc.* **2016**, *138*, 7753.
(44) Ram, M. S.; Riordan, C. G.; Ostrander, R.; Rheingold, A. L. *Inorg. Chem.* **1995**, *34*, 5884.
(45) Vicente, R.; Escuer, A.; El Fallah, M. S.; Solans, X.; Font-Bardia, M. *Inorg. Chim. Acta* **1997**, *261*, 227.
(46) Escuer, A.; Vicente, R.; El Fallah, M. S.; Solans, X.; Font-Bardia, M. *Inorg. Chim. Acta* **1996**, *247*, 85.
(47) Reimer, S.; Wicholas, M.; Scott, B.; Willett, R. D. *Acta Crystallogr., Sect. C: Cryst. Struct. Commun.* **1989**, *45*, 1694.
(48) Burgess, J.; Fawcett, J.; Haines, R. I.; Singh, K.; Russell, D. R. *Transition Met. Chem.* **1999**, *24*, 355.
(49) Crick, I. S.; Hoskins, B. F.; Tregloan, P. A. *Inorg. Chim. Acta* **1986**, *114*, L33.
(50) D'Aniello, M. J.; Mocella, M. T.; Wagner, F.; Barefield, K. E.; Paul, I. C. *J. Am. Chem. Soc.* **1975**, *97*, 192.
(51) Kumar, A.; Periyannan, G. R.; Narayanan, B.; Kittell, A. W.; Kim, J. J.; Bennett, B. *Biochem. J.* **2007**, *403*, 527.
(52) Bennett, B. *Curr. Top. Biophys.* **2002**, *26*, 49.
(53) Jimenez, H. R.; Salgado, J.; Moratal, J. M.; Morgenstern-Badarau, J. *Inorg. Chem.* **1996**, *35*, 2737.
(54) Meier, P.; Merbach, A.; Bürki, S.; Kaden, T. A. *J. Chem. Soc., Chem. Commun.* **1977**, 36.
(55) Martin, R. B. *Biopolymers* **1998**, *45*, 351.
(56) Di, L.; Kerns, E. H.; Fan, K.; McConnell, O. J.; Carter, G. T. *Eur. J. Med. Chem.* **2003**, *38*, 223.
(57) Avdeef, A.; Bendels, S.; Di, L.; Faller, B.; Kansy, M.; Sugano, K.; Yamauchi, Y. *J. Pharm. Sci.* **2007**, *96*, 2893.
(58) Vijay-Kumar, S.; Bugg, C. E.; Cook, W. J. *J. Mol. Biol.* **1987**, *194*, 531.
(59) Beck, M. W.; Oh, S. B.; Kerr, R. A.; Lee, H. J.; Kim, S. H.; Kim, S.; Jang, M.; Ruotolo, B. T.; Lee, J.-Y.; Lim, M. H. *Chem. Sci.* **2015**, *6*, 1879.
(60) Derrick, J. S.; Kerr, R. A.; Nam, Y.; Oh, S. B.; Lee, H. J.; Earnest, K. G.; Suh, N.; Peck, K. L.; Ozbil, M.; Korshavn, K. J.; Ramamoorthy, A.; Prabhakar, R.; Merino, E. J.; Shearer, J.; Lee, J. Y.; Ruotolo, B. T.; Lim, M. H. *J. Am. Chem. Soc.* **2015**, *137*, 14785.
(61) Beck, M. W.; Derrick, J. S.; Kerr, R. A.; Oh, S. B.; Cho, W. J.; Lee, S. J. C.; Ji, Y.; Han, J.; Tehrani, Z. A.; Suh, N.; Kim, S.; Larsen, S. D.; Kim, K. S.; Lee, J.-Y.; Ruotolo, B. T.; Lim, M. H. *Nat. Commun.* **2016**, *7*, 13115.

DOI: 10.1021/jacs.6b09681
J. Am. Chem. Soc. 2017, 139, 2234−2244